Ocean Sci. Discuss., https://doi.org/10.5194/os-2018-167
Manuscript under review for journal Ocean Sci.
Discussion started: 15 February 2019

Impact of wave physics on ocean-wave coupling in CMEMS-IBI Part B : Validation study

Romain Rainaud[(1)], Lotfi Aouf[(1)], Alice Dalphinet[(1)], Marcos Garcia Sotillo[(2)], Enrique Alvarez-Fanjul[(2)], Guillaume Reffray[(3)], Bruno Levier[(3)], Stéphane Law-Chune[(3)], Pablo Lorente[(2)], Cristina Toledano[(4)]

[(1)]Météo-France

[(2)]Puertos del Estado

[(3)]Mercator-Ocean International

[(4)]Nologin Consulting

Abstract

This work aims to evaluate the ocean/waves coupling based on input from the wave model MFWAM. 1-year coupled runs including seasonal variability has been performed for the Iberian Biscay and Ireland domain. We investigated the consequences of improvement in wave physics on the mixed layer of the ocean with a fine horizontal grid size of 1/36°. The ocean model NEMO and the wave model MFWAM have been used for this study to prepare the use of coupling operationally in the IBI Copernicus Marine Service and Monitoring Evironment (CMEMS). Two wave physics versions have been discussed in this study. The validation of sea surface temperature, surface currents have been implemented in comparison with satellite and in-situ observations. The results show a positive impact of the waves forcing on surface key parameters. For storm cases it has been demonstrated a good skill of the ocean/wave coupling to capture the peak of surge event such as the one observed for Petra storm.

Ocean Sci. Discuss., https://doi.org/10.5194/os-2018-167
Manuscript under review for journal Ocean Sci.
Discussion started: 15 February 2019

1. Introduction

Waves act on the interface between the ocean and the atmosphere and have an important role in terms of fluxes exchanges through this interface (Cavaleri et al., 2012). Their representation is necessary to compute with accuracy the different air-sea fluxes of heat and momentum (Janssen et al., 2004). However, waves are generally parameterized from 10-m local winds. While there is a correlation between wind and waves, their relationship is not exclusive. Indeed, waves are also present without wind and for a given local wind speed, the local wave field is variable (Hanley et al., 2010). Moreover, it is generally accepted that wind directly generates surface currents because about 90% of the wind momentum input to waves is immediately passed to the ocean (Cavaleri et al., 2012). In fact, waves absorb energy and momentum from the wind during their formation and growth, and dissipate it when they break (Breivik et al., 2015). This explains why it is necessary to introduce an accurate sea state description, from a wave model (or database as for example Rascle et al., 2008), which controls exchanges between the ocean and atmosphere.

Waves affect the ocean surface layer through different processes (Breivik et al., 2015) :

- Waves induce surface currents via the Stokes drift, rapidly attenuated with depth. The Stokes drift velocity associated with the wave fields adds a term to the Coriolis effect in the momentum equation. This process is called Stokes-Coriolis forcing.
- A part of the atmospheric wind stress is used by waves to grow and is not provided to the ocean. This energy quantity must be subtracted from the oceanic wind stress which drives the ocean model.
- During wave breaking, turbulent kinetic energy is produced and induces an enhanced turbulent mixing in the ocean surface layer.

A more accurate description of these processes will be given in section 2.2.

Recent studies investigated the impact of the wave effect on the representation of the ocean surface layer at different scales of time and space. One of the major impacts is the improvement of the Mixed-Layer Depth (MLD) using a wave-induced MLD parameterisation (Fan et al., 2014) which lead to an important impact on the atmospheric surface temperature, pressure and precipitation (Babanin et al., 2008). In a climate scale, this can affect global sea-surface pressure patterns and atmospheric circulation. Breivik et al., (2015) showed that the use of wave forcing on the oceanic surface lead to reduced global annual SST bias amplitude in the period from 1979 to 2010. They used the NEMO ocean model with a coarse 1° horizontal grid resolution and wave forcing from the ECWAM wave model. A significant decrease of the amplitude of the diurnal cycle

Ocean Sci. Discuss., https://doi.org/10.5194/os-2018-167
Manuscript under review for journal Ocean Sci.
Discussion started: 15 February 2019

of SST and surface currents was shown by Janssen (2012). At the interface between the ocean and atmosphere, waves modify the surface layer and increase the roughness length, which enhances the wind stress (Thévenot et al., 2016). Ginis (2008) suggested the use of an ocean-waves-atmosphere coupled system to improve the representation of tropical cyclone intensity, structure and trajectory. Indeed, Chunxia et al., (2008) studied the effect of sea waves during typhoon Imodu (15-19 July 2003). They found that the waves had a small effect on the typhoon track but they revealed a relation between wage age and 10-m wind speed impacting on air-sea fluxes and precipitation. These changes obviously affect the oceanic surface layer behavior. The high-resolution NEMO-WAM system was used by Staneva et al. (2017) for the Baltic and North Sea. They showed that including wave forcing on the ocean surface leads to a Sea Surface Temperature (SST) closer to the observations provided by the MODIS satellite than without wave forcing. The NEMO-WAM system induced also a better agreement between modeled and observed sea surface height and surface current during Xaver storm event in 6 December 2014.

The Copernicus Marine Environment Monitoring Service (CMEMS) is a relevant European partnership with more than 50 marine operational and research centers in Europe involved in the marine monitoring and forecasting services. It provides a wide range of marine products of social and environmental value such as ocean currents, temperature, salinity, sea level, pelagic biogeochemistry and waves. The Monitoring Forecasting System (MFC) generates model-based products including analysis of the current situation, forecasts of the situation a few days in advance and retrospective data records (re-analyses). In order to increase the quality of these ocean products, an evaluation of the impact of wave forcing on the oceanic surface layer is needed. Météo-France has implemented a coupled system between the wave model MFWAM and the ocean model, NEMO. This aims to provide a reference and an accurate physical oceanic state for the Iberian-Biscay-Ireland (IBI) domain indicated in Figure 1. This work had been done in collaboration with Mercator-Ocean and the Spanish institutions Puertos del Estado, AEMET and CESGA. The goal of this paper is to evaluate the impact of wave forcing on ocean circulation for the IBI region for the year 2014, which had recorded several severe storms events in the east Atlantic ocean. Key oceanic parameters were validated and analysed in preparation for implementing the NEMO v4 IBI-WAVE system in the operational Copernicus CMEMS-IBI-MFC.

This study is split into two parts. The first part was dedicated to the MFWAM validation and was treated in a previous paper. This paper presents the second part, concerned with the impact of wave forcing on the ocean surface and is structured as follows: first, a description of the NEMO ocean model and the coupling processes is given in section 2. Section 3 consists of a review of the different observations and experiments performed. Results of the impact of the ocean-wave coupling and comparisons with observations are given in Section 4. Finally, a summary and concluding remarks are discussed in Section 5.

2. Model Description

2.1. The NEMO ocean model

The NEMO-IBI numerical core is based on the NEMO v3.6 ocean general circulation model (Madec, 2008). This model solves the three-dimensional finite difference primitive equations, assuming the hydrostatic equilibrium and Boussinesq approximation. These equations are discretized on a 1/36° (~2-3 km) horizontal resolution ORCA grid and 50 z-streched vertical levels, with a resolution decreasing from ~1 m in the upper ocean to more than 400 m in the deep ocean. The domain covers the IBI area representing the Northeast Atlantic Ocean from the Canary Islands to Iceland and from 20°W to 10°E, with open boundaries on the four sides (Figure 1) : West at 20°W, North at 63°N, South at 25°N and East at 10°E enclosing Kattegat Strait and the Western Mediterranean Sea from the Gulf of Genoa to Tunisia. The lateral open boundary conditions are provided by Mercator Ocean's PSY4V3R1 daily analysis product at a 1/12° (~10-12 km) resolution. These are complemented by 11 tidal harmonics (M2, S2, N2, K1, O1, M4, K2, P1, Mf, Mm) built from FES2004 (Lyard et al., 2006) and TPX07.1 (Egbert and Erofeeva, 2002) from tidal model.

The turbulent mixing scheme uses the parameterizations and equations from Warner et al. (2005). Vertical turbulent processes are parameterized with a k-epsilon two-equation model implemented in the generic form proposed by Umlauf and Burchard (2003). The advection of tracers is computed with the QUICKEST scheme (Leonard 1979) connected to the limiter of Zalezak (1979). This third-order scheme is well suited to high resolution used here and modeling of the sharp fronts characteristic of coastal environments.

Fresh water river discharge inputs are implemented as lateral boundary conditions for 33 rivers. Flow rate data are based on daily observations (for 9 of the rivers, gathered in the PREVIMER project), simulated data from the SMHI E-HYPE hydrological model (http://e-hypeweb.sms.se) and climatology from the Global Runoff Data Centre (http://www.bafg.de/GRDC) and the French hydrographic database « Banque Hydro » (http://hydro.eaufrance.fr). Rivers are applied by specifying a constant velocity in the vertical, and Neumann conditions for temperature and constant salinity (0.1 psu).

2.2. Coupling processes

The impact of the waves field on the upper ocean layer is driven by the following three physical processes (Figure 2, Breivik et al. 2015):

- Stokes-Coriolis forcing: it is generally the dominant source of wind-correlated drift of surface waters, but also the source of mixing in the upper ocean by Langmuir circulation (Rascle and Ardhuin 2013). Stokes velocity components (v_s) are computed by the MFWAM model and provided to the NEMO model. They interact with the Coriolis force to produce an additional forcing on the momentum:

$$\frac{Du}{Dt}=-\frac{1}{\rho_w}\nabla p+(u+v_s)\times f\vec{z}+\frac{1}{\rho_w}\frac{\partial\tau_{oc}}{\partial z}$$

With ρ_w the water density, p the pressure, f the Coriolis factor, u the Eulerian current, z the vertical positive coordinate (positive up) and τ_{oc} the surface wind stress.

- The second process is the net surface wind stress due to wave growth: the waves grow and absorb energy provided by the wind stress. The wind stress left to the ocean is the difference between the total wind stress and that consumed by the waves. The MFWAM model provides NEMO with the neutral drag coefficient and the ratio (named coeffstress) between the ocean surface wind stress (τ_{oc}) and the total atmospheric wind stress (τ_a). This ratio is used to compute the ocean wind stress as given by the following relation :

$$\tau_{OC}=\tau_A\times coeffstress$$

- The third process is the Turbulent Kinetic Energy (TKE) induced by wave breaking. As the waves break at the ocean surface, a flux of turbulent kinetic energy is released to the ocean. This energy flux Φ_{oc} is computed by the dissipation source term in MFWAM. Craig and Banner (1994) parameterized the energy flux with a non-dimensional relation depending on the friction velocity as indicated here below :

$$\Phi_{OC}=\frac{\rho_a^{3/2}}{\rho_w^{1/2}}\alpha_{CB}u^{*3}$$

Ocean Sci. Discuss., https://doi.org/10.5194/os-2018-167
Manuscript under review for journal Ocean Sci.
Discussion started: 15 February 2019

Ocean Science Discussions

Where ρ_a and ρ_w are the air and water density, respectively, u* is the air side friction velocity and α_{CB} is the Craig and Banner parameter. As Φ_{oc} is computed by MFWAM, α_{CB} can be deduced from the Craig and Banner parameterisation.

3. Observations and experiments

3.1 In situ observations

Satellite data

Two different SST satellite products, OSTIA and L3S, have been used in this study. The OSTIA daily product of SST is a level 4 multi-sensor product at a resolution of 0.02° built by using optimal interpolation from several satellite missions such as AVHRR_METOP_B, SEVIRI*VIIRS_NPP, AVHRRL_19, AVHRRL_18, MODIS_A, MODIS_T, AMSR2. The hierarchy can be changed depending on the health of each sensor. The L3S product consists of a fusion of daily SST observations from multiple satellite sensors, over a 0.1° resolution grid. It includes observations by polar orbiting (NOAA-18 & NOAA-19/AVHRR, METOP-A/AVHRR, ENVISAT/AATSR, AQUA/AMSRE, TRMM/TMI) and geostationnary (MSG/SEVIRI,GEOS-11) satellites. The observations of each sensor are intercalibrated prior to merging using a bias correction based on a multi-sensor median reference correcting the large scale cross-sensor biases.

Satellite observations of significant wave height (SWH) for the year 2014 are provided by the JASON-2 and SARAL altimeters. Altimeter SWHs are interpolated in a box with a grid size of 0.1° and collocated with MFWAM's modelled SWH with a time window of 3 hours.

Level 4 surface current satellite data are from satellite altimeter gridded sea surface heights and derived variables. This product is processed by the SL-TAC multimission altimeter data processing system. It processes data from all altimeter missions: Jason-3, Sentinel-3A, HY-2A, Saral/AltiKa, Cryosat-2, Jason-2, Jason-1, T/P, ENVISAT, GFO, ERS ½. It provides a consistent and homogeneous catalogue of products for varied applications, both for near real time applications and offline studies. The resolution of the product is 0.25°.

Moored buoys

In-situ buoys are also used to evaluate model outputs. These buoys provide data of near-surface atmosphere, wave and ocean parameters. Data are provided from the Puertos del Estado network buoys, Meteo France buoys and Marine institute network of buoys. The Table 1 and Figure 1 summarize the names, locations, nationality and reference codes used in the following for the different buoys.

3.2. Ocean experiments

Three ocean experiments have been performed to evaluate the impact of the wave forcing on the IBI area. The first experiment was perfomed without wave forcing, and is called NEMO-Ref. The other two ocean experiments were implemented with wave forcing provided by the model MFWAM V3 and V4, and are called NEMO-WaveV3 and NEMO-WaveV4, respectively.

The ocean experiments covered the same period as the wave model run. Initial conditions were provided by Mercator-Ocean from a free run started on 23rd February, 2013. The atmospheric forcing was provided by the ECMWF atmospheric system. 10-m wind speed, surface pressure, 2-m temperature and relative humidity were provided with a 3h period (analysis at 0 and 12UTC, forecasts at 3-6-9 and 15-18-21UTC) and a 1/12° (~12 km) horizontal resolution. Evaporation, latent and sensible heat fluxes and wind stress for NEMO-Ref were computed using the CORE parameterization (Large and Yeager 2004).

NEMO-WaveV3 and NEMO-WaveV4 have the same configuration as NEMO-Ref in term of initial and boundary conditions and atmospheric forcing. However, a surface-wave forcing was provided every 3 hours from outputs of MFWAM-V3 for NEMO-WaveV3 and from outputs of MFWAM-V4 for NEMO-WaveV4. In both experiments, all wave processes described in section 2.2 were activated.

4. Results of the ocean-wave coupling

4.1. Impact of wave forcing on the ocean surface

Wave impact for 2014

The wave impact on the ocean surface layer was first evaluated for the year 2014 by comparison between ocean surface parameters from NEMO-Ref, NEMO-WaveV4 and NEMO-WaveV3. The validation of the results was performed by comparison with the observations.

Figure 3a shows the mean of Sea Surface Temperature (SST) from NEMO-Ref during 2014. This is characterized by a South-North gradient, with a maximum of 22°C in the Canary islands and a minimum of 4°C in the Baltic Sea. During the year 2014, the mean SST field from NEMO-WaveV4 remains close to that of NEMO-Ref. Indeed, Figure 3b shows the difference between these two experiments and reveals some patches of difference on the IBI domain but not exceeding a value of 0.5°C. SST from NEMO-WaveV4 is colder or warmer than NEMO-Ref in these patches. The difference of SST between NEMO-WaveV3 and NEMO-WaveV4 also shows patches of absolute value of 0.3°C over the entire domain, as illustrated in figure 3c. NEMO-WaveV3 is alternately colder and warmer than NEMO-WaveV4.

The mean Sea Surface Salinity (SSS) field from NEMO-Ref for 2014 has two South-North gradients, as illustrated in figure 4a. The first gradient is located in the Atlantic Ocean ranging from 37 psu in the Canary islands to less than 34 psu in the Baltic Sea. The second gradient is observed in the Mediterranean Sea ranging from 36 psu along the North-African coast to 39 psu in the Gulf of Lion. The impact of wave forcing on salinity is mainly observed at the Danish coast where SSS from NEMO-WaveV4 is greater than NEMO-Ref by roughly 0.8 psu. However along the Scandinavian coast SSS from NEMO-WaveV4 is lower than NEMO-Ref by 0.4 psu. In this region it seems that there has been a significant impact related to wave forcing from MFWAM-V4. Figure 4c shows that SSS from NEMO-WaveV3 is greater than SSS from NEMO-WaveV4 by 0.6 psu along the Scandinavian coast and lower by 0.4 psu along the Danish coast. Elsewhere there is no noticeable difference of SSS induced by the version of model MFWAM.

Figure 5a and 6a show the surface current fields (U and V components), where we can easily see several mesoscale structures in the deep water domain, i.e. beyond the Western European continental slope. Differences with NEMO-WaveV4 can be seen in these structures, as illustrated in figures 5b and 5c. Indeed, the presence of dipoles of 0.2 m/s intensity shows that the wave forcing slightly modifies the location of these mesoscale structures. These dipoles are also different between NEMO-WaveV3 and NEMO-WaveV4, as shown in figures 5c and 6c. This means that the change in the wave forcing has had a direct affect on the location of the mesoscale structures.

The mean turbocline for 2014 in NEMO-Ref is below 200 m for the entire domain except in the north-west, between Ireland and Iceland, where the Turbocline is at roughly 400 m, as illustrated in figure 7a. In this area the differences with NEMO-WaveV4 are roughly +/- 40 m, as indicated in figure 7b. However in the rest of the domain, there is no impact by the wave forcing. Figure 7c shows also that the largest difference between NEMO-WaveV3 and NEMO-WaveV4 occurs between Ireland and Iceland. There are several dipoles with differences of +/- 20 m, which basically follow those of surface current shown in figure 6.

Surface fields from NEMO can be compared with satellite observations for 2014. Figures 8 shows the difference of SST between the NEMO runs and the OSTIA data. For all NEMO runs, the differences between fields are globally similar and show a good agreement with the OSTIA SST during the year 2014. There are patches of difference of absolute value of 0.5°C which indicate that SST from the NEMO simulations are colder. There are more patches observed with NEMO-WaveV3 and NEMO-WaveV4 than NEMO-Ref. A cold spot at the Strait of Gibraltar of -1.8°C and hot strings of 0.6°C along the Spanish and Moroccan coasts are also seen for the three experiments. Statistical parameters between NEMO and OSTIA are shown in Table 2. This confirms the cold SST bias for the NEMO runs. The bias of NEMO-Ref is slightly smaller than for the other runs, while the smallest RMS error is obtained from NEMO-WaveV4. NEMO-WaveV4's enhanced performance relative to NEMO-WaveV3 reflects the improvement in the MFWAM-V4 physics. The same trend has been found for the comparisons of the spatial distribution of SST from the L3S satellite product, shown in Table 2.

Figures 9a and 9b describe the monthly variation of SST bias and RMS error , respectively. Except in June, the three NEMO simulations are colder than the OSTIA satellite data. In winter, the NEMO-Ref simulation scores slightly better than the wave-forced simulations. During the rest of the year, scores for all simulations are very similar. Simulations with wave coupling are sometimes better than NEMO-Ref. Note also that NEMO-WaveV3's bias is always colder than NEMO-WaveV4's. RMS is also always lower for NEMO-WaveV4 compared with NEMO-WaveV3, but close to NEMO-Ref, except for November and December 2014.

Surface currents from the NEMO runs are now compared with L4 satellite products. Figure 10 show that for all NEMO experiments, NEMO represents well the surface current velocity in the global IBI domain, except in a few areas. There is an underestimation of almost 0.5 m/s of the surface current velocity along the English Channel and southern coasts of the North Sea. There are patches of difference approaching the Bay of Biscay's shelf where NEMO underestimates surface currents by roughly 0.2 m/s. In contrast, in the Mediterranean Sea the NEMO runs overestimate surface currents by roughly 0.3 m/s. Comparing figures 10a and 10b shows that surface currents of NEMO-WaveV4 are slightly closer to the L4 currents than NEMO-Ref, especially in the North Sea and the Bay of Biscay. On the other hand, a comparison of figures 10b and 10c shows that wave forcing from MFWAM-V4 improves the quality of surface currents. Indeed, patches of underestimation are smaller for NEMO-WaveV4 than for NEMO-WaveV3. The scores showed in Table 3 confirm the very good performance of NEMO in term of surface currents despite a slight underestimation, the improvement of surface current representation using wave forcing and the improvement by MFWAM-V4 physics.

In other respects we focus on the comparison between NEMO-WaveV4 and NEMO-Ref. Daily currents are compared with observations from moored buoys during 2014 (see Table 1 for locations and names of the buoys). Figure 11 shows

the scatter index of surface currents at the GCan buoy during 2014. A good agreement is found between model and observations for NEMO-Ref and NEMO-WaveV4, especially for low currents of around 0.2 m/s. However the dispersion can be significant, with a SI of around 70% for the two runs. Scores in Table 4 show that NEMO-Ref and NEMO-WaveV4 alternate in how close they agree with the buoys' data. For example, at the CPal buoy, NEMO-WaveV4 is is less biased and has a lower RMS than NEMO-Ref while the opposite is true at the Vale buoy. Moreover, Table 4 shows that the RMS error of surface current scores are generally under 0.1 m/s, illustrating the good performance of the NEMO-IBI model, with or without wave forcing.

Wave Impact during Storm Hercules

Storm Hercules occurred on the 6th January 2014 and was characterized by significant wave height of roughly 14 m in the Atlantic Ocean, close to the southwestern off shore of Ireland (Figure 12). During this event, in NEMO-Ref the wind stress was around 0.6 N/m^2 at the storm location, reaching a maximum of 0.9 N/m^2 (Figure 13a). The wind stress calculated in NEMO-WaveV4 was greater by almost 0.16 N/m^2 at the storm location and was similar outside of the storm (Figure 13b). This input of momentum first slightly cooled the surface by almost 0.2°C at the storm location (Figure 13c). Moreover, the impact of wave forcing during this event is particularly characterized by an enhancement of of the surface current of roughly 0.4 m/s for U component at the storm location (Figure 13d). In order to minimize altimeter artifacts which can produce some unexpected biases, the L4 and NEMO currents are daily averaged in January for the comparisons between model and observations. Comparisons with L4 currents (Figure 14) show some patches of underestimation between -0.2 m/s and -0.4 m/s at the storm location for NEMO-Ref. These patches are not found in the comparison with NEMO-WaveV4. For this experiment, even if there are some dipoles of difference (0.1 m/s), L4 currents and NEMO-WaveV4 currents are overall close. However, an overestimation is observed in the time series for the buoys affected by the storm (Figure 15b). The Table 5 shows the scores of surface current during Hercules's passage throughout the IBI domain (compared with the L4 satellite currents) and at the moored buoys impacted by the storm. As with the time series, currents are overestimated at the moored buoy locations, more so for NEMO-WaveV4. However, on the global IBI domain, NEMO-WaveV4's bias is close to null while NEMO-Ref underestimates the surface current by almost 30%.

Wave impact during Storm Petra

Storm Petra occurred on the 5th February 2014 and was characterized by significant wave heights of almost 13 m affecting the Brittany coast of France (Figure 16). At the storm location, the wind stress in NEMO-Ref reached 0.9 N/m^2 (Figure 17a). As with Storm Hercules, wind stress in NEMO-WaveV4 is greater than in NEMO-Ref - especially at the storm location – with values between 0.08 and 0.16 N/m^2 (Figure 17b). In the area surrounding the storm, wind stress in both experiments is equivalent. The impact of these mechanical energy input differences on oceanic parameters is broadly the same as for Hercules. Figure 17c and Figure 17d show differences between NEMO-WaveV4 and NEMO-Ref for the daily averaged SST and U-component of surface current. The wave forcing produces a slight cooling of the surface of almost 0.2°C, due to a combination of vertical mixing and heat extraction by the atmosphere, and a significant increase of almost 0.4 m/s at the storm location. Comparisons with moored buoys over which Petra passed show that for this event NEMO at turns underestimated and overestimated surface current. Indeed, at the Bilb buoy (Figure 18a), NEMO underestimates surface current and NEMO-WaveV4 is in better agreement with measurements. On the contrary, for the CSil buoy (Figure 18b), NEMO-Ref is in good agreement with measurements while NEMO-WaveV4 overestimates surface current. As for Hercules, February surface currents from the L4 satellite and NEMO experiments are averaged for comparison. (Figure 19). We can see some patches of underestimation (between -0.2 m/s and -0.5m/s) of surface currents in NEMO-Ref, while there are some patches of overestimation (between 0.3 m/s and 0.4 m/s) of surface currents by NEMO-WaveV4. Table 6 summarizes scores between the NEMO experiments, L4 satellite currents and buoys impacted by Petra. In general, throughout the IBI domain, NEMO-WaveV4 surface currents are very close to the L4 satellite while NEMO-Ref underestimates the current by almost 25%. However, surface currents computed by NEMO-WaveV4 at buoy locations are greater than those of NEMO-Ref. NEMO-Ref performs better at the CSil and EBar buoys and NEMO-WaveV4 performs better at the Bilb buoy. The impact of the wave forcing during Petra is also investigated for the sea surface height (SSH) using measurements at the moored buoys Le Crouesty (Figure 20a) and Fishguard (Figure 20b). The SSHs of the two NEMO experiments are similar and slightly lower than observations when SSH is lower than 0.20 m.. However, these time series show the improvement with the wave coupling of the peaks of SSH during the storm. Indeed, at the two buoys, storm induced peaks of SSH (almost 0.80 m in observations) are better represented by NEMO-WaveV4 than NEMO-Ref.

4.2. Sensitivity to the modification of atmospheric forcing by waves

In this section we investigate the sensitivity of the surface oceanic fields to the modification of atmospheric forcing by waves. To this end, additional run NEMO-Wave V4 was performed with not accounting of the neutral drag coefficient and the ratio between oceanic and atmospheric wind stress. This coupled run is called NEMO-WaveV4-NoAtm which uses then the default bulk relation in NEMO model for the momentum and heat fluxes. The surface fields of NEMO-WaveV4 and NEMO-WaveV4-NoAtm are compared to evaluate the effect of waves on the stress forcing.

First, the comparison of wind stress between the two experiments is shown in Figure 21a. Wind stress from NEMO-WaveV4 is slightly higher (almost by 0.1 N/m^2) from the Bay of Biscay to the northern boundary of the domain. In the rest of the IBI domain the wind stresses are similar.

Concerning SST difference illusyrated in Figure 21b, we observed some patches in the Atlantic ocean near the Portuguese coast where NEMO-WaveV4-NoAtm is warmer by almost 0.5°C. On the contrary, in the Mediterranean Sea, NEMO-WaveV4-NoAtm is locally cooler by almost 0.5°C. We can mention also the presence of a dipole of difference of almost 1°C in the Strait of Gibraltar. The difference in drag coefficient affect significantly the heat fluxes and therefore explains warmer SST in he Atlantic ocean from run NEMO-WaveV4-NoAtm.

Figure 21c shows a very weak impact on SSS. Indeed, the effect on SSS of atmospheric forcing modification by waves is only along the Scandinavian coasts and in some places in the Mediterranean Sea and Bay of Biscay. In these areas, there are some patches of SSS of NEMO-WaveV4-NoAtm almost 0.4 psu lower; this is also in part due to a combination of vertical mixing with deeper water and moisture exchanges with atmosphere.

Figures 21d and 21e present the effect on U- and V-components of surface currents. Here again, the impact is mainly on mesoscale structures. Dipoles of differences of almost +/-0.2 m/s are due to the modification of these structure's locations.

For the Turbocline (Figure 21f), differences between both experiments are localized between Ireland and Iceland. In this area, the turbocline of NEMO-WaveV4 is deeper by almost 30 m, following the pattern of differences on surface wind stress (Figure 21a).

There is a good agreement between yearly means of model SST and satellite SST from OSTIA L4 and L3S . However, NEMO-WaveV4-NoAtm shows cooler temperature than observations by almost 0.6°C near the British coast and in the Mediterranean Sea. We can also mention that the cold pool in the Strait of Gibraltar observed from runs NEMO-Ref and NEMO-WaveV4 (Figure 8 a) is not revealed. Differences in surface currents between NEMO-WaveV4-NoAtm and L4 currents are very similar to the difference between L4 currents and NEMO-WaveV4. Table 7 shows the statistical parameters for all runs in comparison with satellite SST. NEMO-WaveV4-NoAtm has better scores compared with NEMO-WaveV4 and NEMO-Ref for both satellite products. This shows that in NEMO-WaveV4, the atmospheric forcing modification by waves overestimates the surface cooling. However, for the surface currents, the atmospheric forcing reduces the difference with L4 currents and improves the scores, especially the bias.

5. Conclusions

The impact of Stokes-Coriolis forcing, the wind stress due to wave growth and the wave breaking in NEMO ocean model on IBI domain has been evaluated through a 1-year simulation in 2014. Two wave forcing from wave physics settings of from the model MFWAM V3 and V4 have been compared to investigate the impact on ocean circilation..

The impact of wave forcing on sea surface temperature can reach 0,5°C in average on some areas, negatively or positively. The changes on the wave model configuration is quite sensitive with impacts of 0,3°C. Noticeable differences induced by the version of model MFWAM were also observed on salinity at the Danish and Scandinavian coast and on the surface currents of the mesoscale circulation.

The NEMO-Wave V4 shows its good representation of ocean surface with the smallest RMS error in comparison with OSTIA Level 4 data. Also we observed a slightly better fit to L4 surface currents than the ones obtained from NEMO-Ref run. This performance is enhanced comparing to NEMO-Wave V3 thanks to the improvement in the MFWAM physics. However the cold bias is more important than in NEMO-Ref.

The simulation of the models has been evaluated during two North Atlantic storms, Hercules and Petra. The wave forcing during both storms induces an increase of of surface currents at the storm locations. This has been validated by satellite observations for Hercules. During Petra, NEMO-Wave V4 overestimates satellite measurements of surface currents as much as NEMO-Wave V3 underestimate them.

In other respects we have demonstrated a better sea surface heights at the peak of storm when using the wave forcing in NEMO run.

The coupling runs have showed the good performance of the wave forcing in NEMO model, with slight improvement on sea surface temperature and surface currents. The oceanic outputs are modified during storm and also on the first layers with perturbation of the mesoscale structures and possible modifications of the thermocline. The impact of waves on the atmospheric forcing remains an issue and additional investigations are needed. In other respects, the assimilation of satellite altimeters wave data will step forward to a better wave forcing for ocean circulation model. This will be conducted in the frame of the phase 2 of the Copernicus marine service CMEMS-IBI.

Ocean Sci. Discuss., https://doi.org/10.5194/os-2018-167
Manuscript under review for journal Ocean Sci.
Discussion started: 15 February 2019

Ocean Science Discussions
Open Access

6. References

Ardhuin, F., Rogers E., Babanin A., Filipot J-F., Magne R., Roland A., Van der Westhuysen A, Queffeulou P., Lefevre J.-M., Aouf L., Collard F. : Semi-empirical dissipation source functions for wind-wave models: part I, definition, calibration and validation, Journal of Physical Oceanography, Volume 40, pp1917-1941, https://doi.org/10.1175/2010JPO4324.1, 2010.

Babanin, A., Onorato M., Qiao, F. : Surface waves and wave-coupled effects in lower atmosphere and upper ocean, *Journal of Geophysical Research.*, 117, C11, https://doi.org/10.1029/2012JC007932, 2012.

Babanin, A. V., Ganopolski A., Phillips W. R. C. : Wave-induced upper-ocean mixing in a climate model of intermediate complexity. *Ocean Modelling*, **29**, 189–197, https://doi.org/10.1016/j.ocemod.2009.04.003, 2009.

Breivik, O., Mogensen K., Bidlot J., Balmaseda M., Janssen P. : Surface wave effects in the NEMO ocean model : Forced and coupled experiments, Journal of Geophysical Research, Volume 120, issue 4, 2973-2992, https://doi.org/10.1002/2014JC010565, 2015.

Cavaleri, L., Fox-Kemper B., Hemer M. : Wind waves in the climate coupled system. Bulletin of American Meteorlogical Society, 1651-1661, https://doi.org/10.1175/BAMS-D-11-00170.1, , 2012.

Chunxia L., QuanqI Y., Liang L. : The effect of sea waves on the typhoon Imodu, Proceeding of High Resolution Modelling CAWCR workshop, Melbourne, Australia, 25-28 November 2008.

Egbert, G. D., Erofeeva, S. Y., : Efficient inverse modelling of barotropic ocean tides, Journal of Atmospheric and Oceanic Technology, **19**, 183–204, **19**, 183–204, https://doi.org/10.1175/1520-0426(2002)019<0183:EIMOBO>2.0.CO;2 2002.

Fan, Y., and S. M. Griffies S. M. : Impacts of parameterized Langmuir turbulence and nonbreaking wave mixing in global cli-mate simulations. Journal of Climate, 27, 4752–4775, https://doi.org/10.1175/JCLI-D-13-00583.1, 2014

Ginis, I. : Atmophere-Ocean coupling in tropical cyclone, Proceedings of ECMWF workshop on Ocean-Atmosphere interactions, Reading, UK, 10-12 November, 2008.

Hanley, K. E., Belcher S. E., Sullivan P. P. : A global climatology of wind-wave interaction. *J. Phys. Oceanogr.*, 40, 1263–1282, https://doi.org/10.1175/2010JPO4377.1, 2010.

Janssen, P. A. E. M., 2004 : The Interaction of Ocean Waves and Wind. Cambridge University Press.

Janssen, P. A. E. M. : Ocean wave effects on the daily cycle in SST, *J. Geophys. Res.*, 117, C00J32, https://doi.org/10.1029/2012JC007943, 2012.

Ocean Sci. Discuss., https://doi.org/10.5194/os-2018-167
Manuscript under review for journal Ocean Sci.
Discussion started: 15 February 2019

Leonard, B. P., : A stable and accurate convective modelling procedure based on quadratic upstream interpolation, Computer Methods in Applied Mechanics and Engineering, 19, issue 1, 59-98, https://doi.org/10.1016/0045-7825(79)90034-3 1979.

Lyard, F., Lefèvre, F., Letellier, T., Francis, O., : Modelling the global ocean tides : modern insights from FES2004, Ocean Dynamics, 56, issue 5-6, 394-415, https://doi.org/10.1007/s10236-006-0086-x 2006.

Rascle, N., Ardhuin, F., Queffeulou, P., Croiz´e-Fillon, D. : A global wave parameter database for geophysical applications. Part 1: wave-current-turbulence interaction parameters for the open ocean based on traditional parameterizations. Ocean Modelling 25, 154–171,https://doi.org/10.1016/j.ocemod.2008.07.006, 2008.

Staneva J., Alari V., Breivik O, Bidlot J.-R. and Mogensen K. : Effects of wave-induced forcing on a circulation model of the North Sea. Ocean Dynamics, Vol. 67, Issue 1, 81-191, https://doi.org/10.1007/s10236-016-1009-0, 2017

Thevenot, O., M-N. Bouin, V. Ducrocq, C. Lebeaupin-Brossier, O. Nuissier, J. Pianezze, F. Duffourg : Influence of the sea state on Mediterranean heavy precipitation : A case study from Hymex-SOP-1, Quarterly Journal of the Royal Meteorological Society, Volume 142, Issue S1, Pages 377-389, http://doi.org/10.1002/qj.2660, 2016.

Zalezak, S. T., : Fully multidimensional flux-corrected transport algorithms for fluids. J. Comput. Phys. 31: 335–362. https://doi.org/10.1016/0021-9991(79)90051-2,1979.

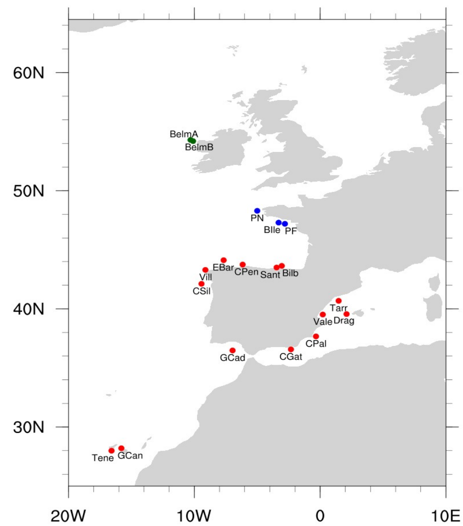

Figure 1 : Name and location of buoys in the IBI domain.

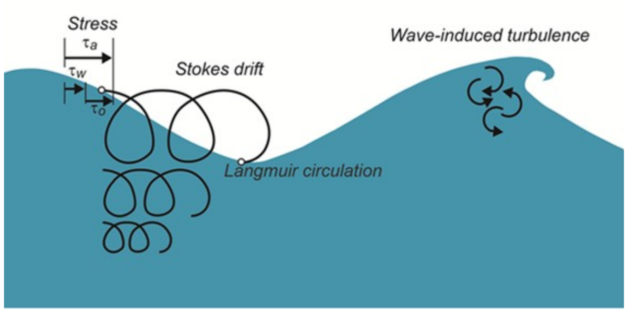

Figure 2 : Schematic of the physical processes involved in the wave's impact on the oceanic surface layer (from Breivik et al., 2015).

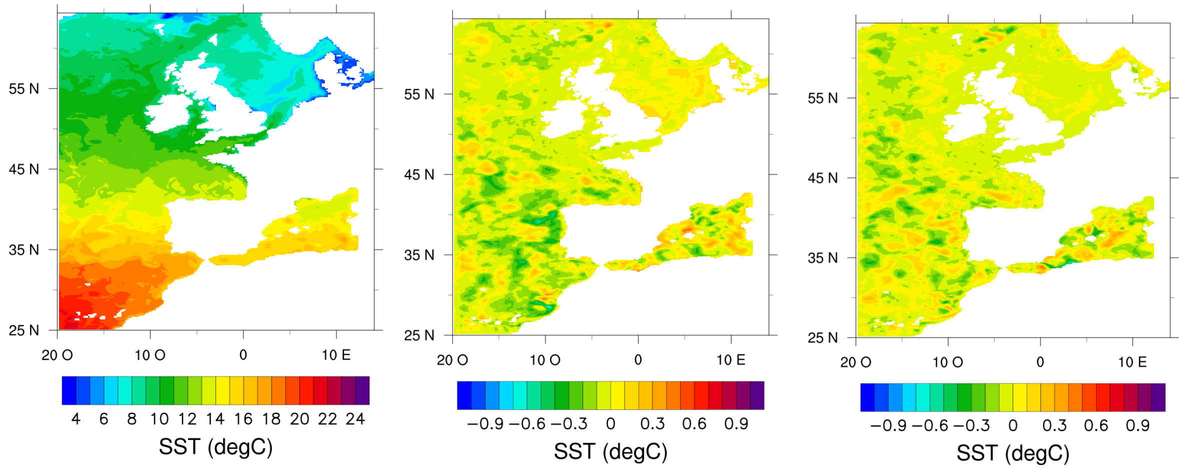

(a) (b) (c)

Figure 3 : Mean 2014 SST fields on the IBI domain from (a) NEMO-Ref, (b) NEMO-WaveV4 – NEMO-Ref and (c) NEMO-WaveV3 – NEMO-WaveV4.

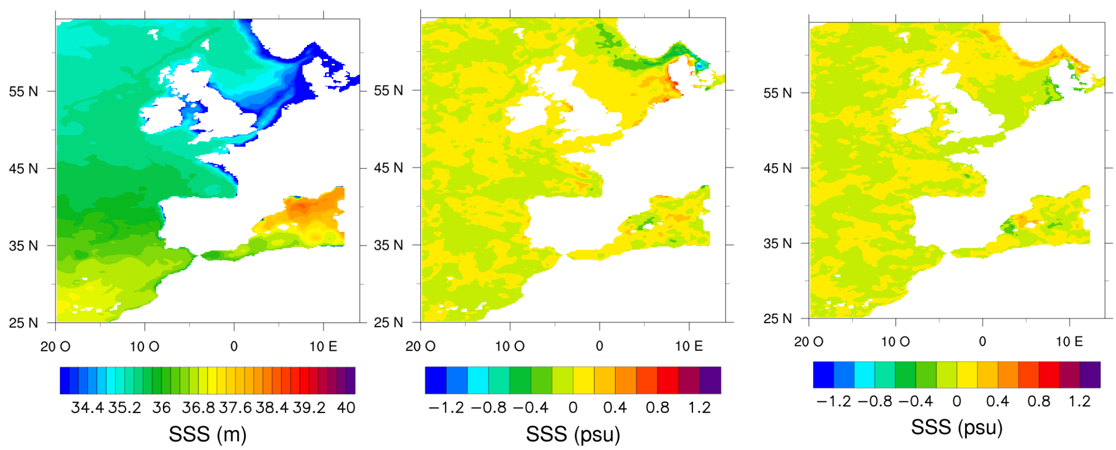

(a) (b) (c)

Figure 4 : Mean 2014 SSS fields on the IBI domain from (a) NEMO-Ref, (b) NEMO-WaveV4 – NEMO-Ref and (c) NEMO-WaveV3 – NEMO-WaveV4.

Ocean Sci. Discuss., https://doi.org/10.5194/os-2018-167
Manuscript under review for journal Ocean Sci.
Discussion started: 15 February 2019

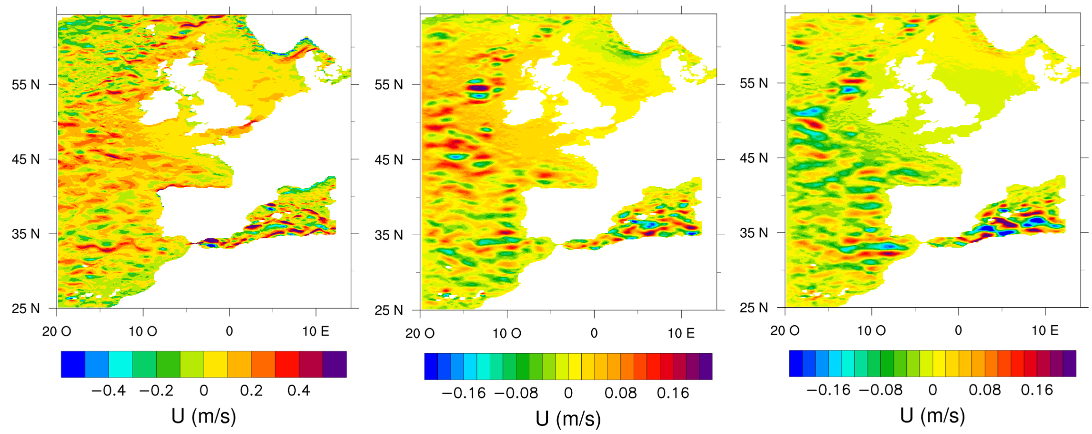

(a) (b) (c)

Figure 5 : Mean 2014 fields of U-component of surface currents on the IBI domain from (a) NEMO-Ref, (b) NEMO-WaveV4 – NEMO-Ref and (c) NEMO-WaveV3 – NEMO-WaveV4.

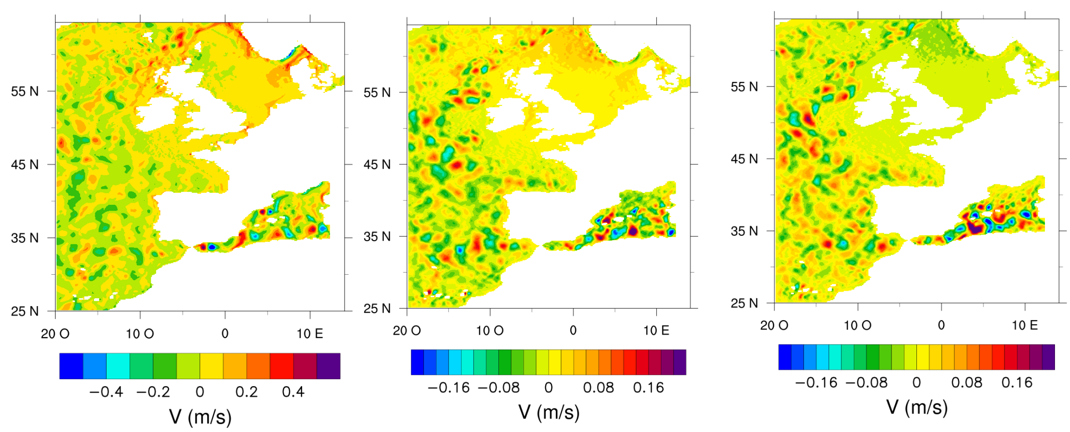

(a) (b) (c)

Figure 6 : Mean 2014 fields of V-component of surface currents on the IBI domain from (a) NEMO-Ref, (b) NEMO-WaveV4 – NEMO-Ref and (c) NEMO-WaveV3 – NEMO-WaveV4.

Ocean Sci. Discuss., https://doi.org/10.5194/os-2018-167
Manuscript under review for journal Ocean Sci.
Discussion started: 15 February 2019

Ocean Science Discussions
Open Access
EGU

(a) (b) (c)

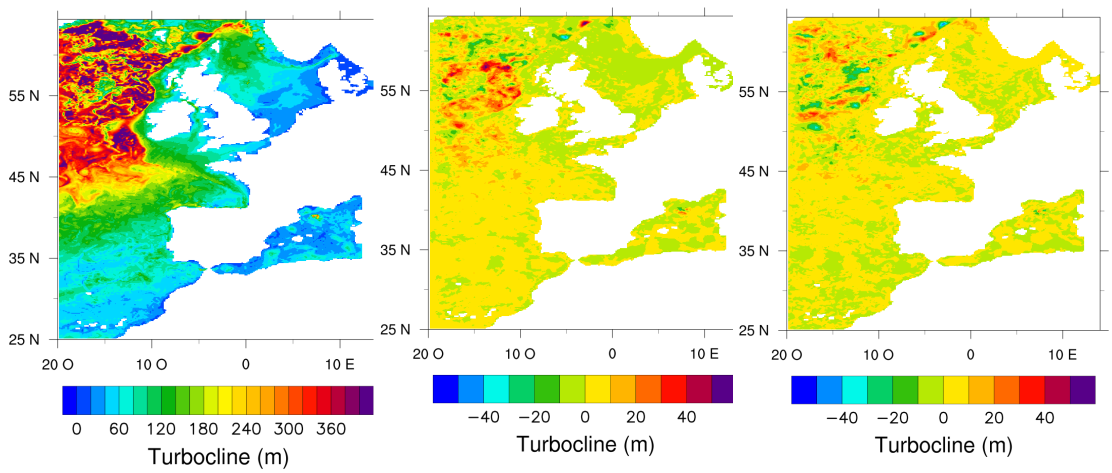

Figure 7 : Mean 2014 Turbocline fields on the IBI domain from (a) NEMO-Ref, (b) NEMO-WaveV4 – NEMO-Ref and (c) NEMO-WaveV3 – NEMO-WaveV4.

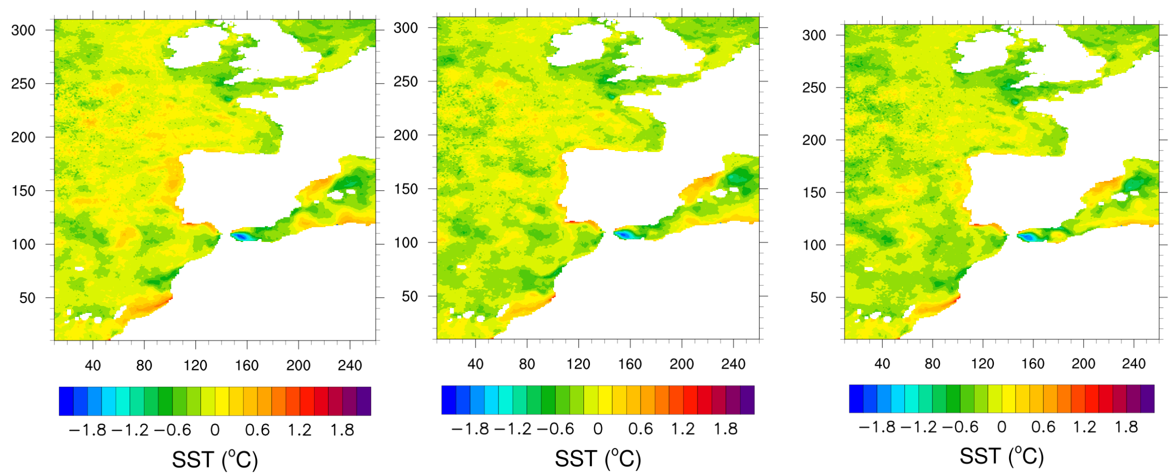

(a) (b) (c)

Figure 8 : SST fields averaged on 2014 of differences between NEMO and OSTIA for (a) NEMO-Ref, (b) NEMO-WaveV4 and (c) NEMO-WaveV3.

Ocean Sci. Discuss., https://doi.org/10.5194/os-2018-167
Manuscript under review for journal Ocean Sci.
Discussion started: 15 February 2019

Ocean Science
Discussions
Open Access

(a)

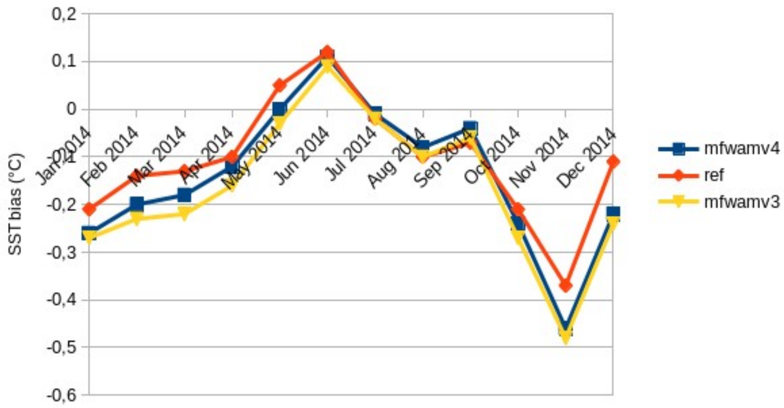

(b)

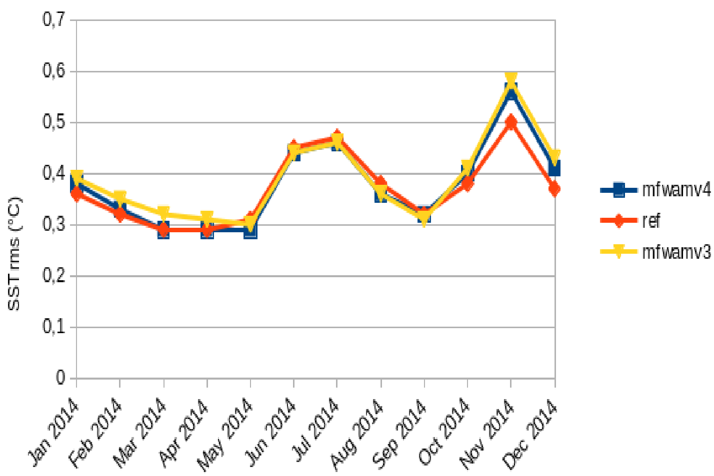

Figure 9 : Monthly evolution of (a) bias and (b) RMS between NEMO and OSTIA SST. Blue lines with squares are for NEMO-WaveV4, orange lines with diamonds are for NEMO-Ref and yellow lines with triangles are for NEMO-WaveV3.

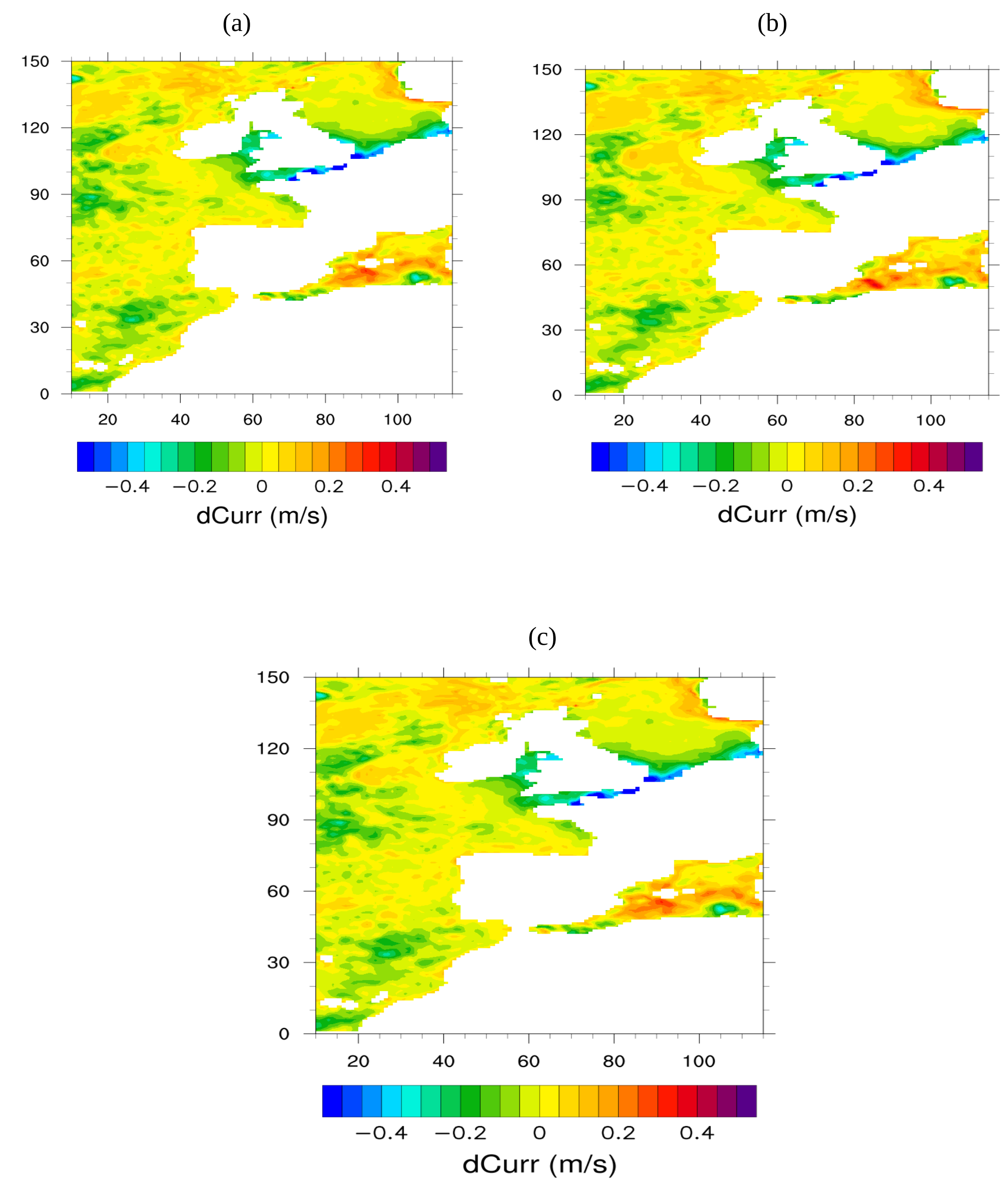

Figure 10 : Mean differences of surface current velocity during 2014. (a), (b) and (c) stand for NEMO-Ref - L4 surface currents, NEMO-WaveV4 – L4 surface currents and NEMO-WaveV3 – L4 currents, respectively.

Ocean Sci. Discuss., https://doi.org/10.5194/os-2018-167
Manuscript under review for journal Ocean Sci.
Discussion started: 15 February 2019

Ocean Science
Discussions
Open Access

(a)

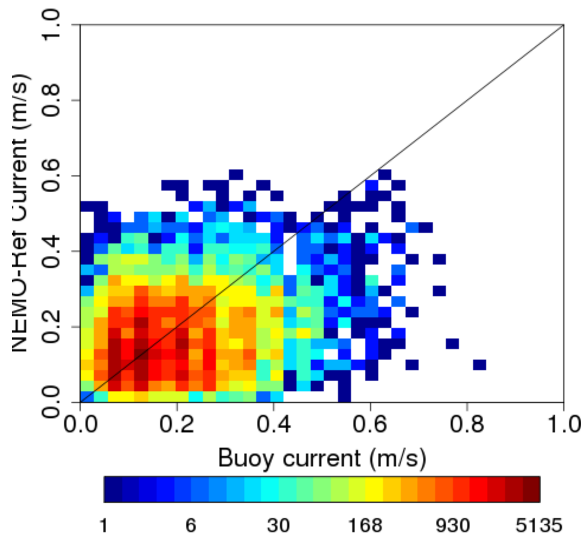

(b)

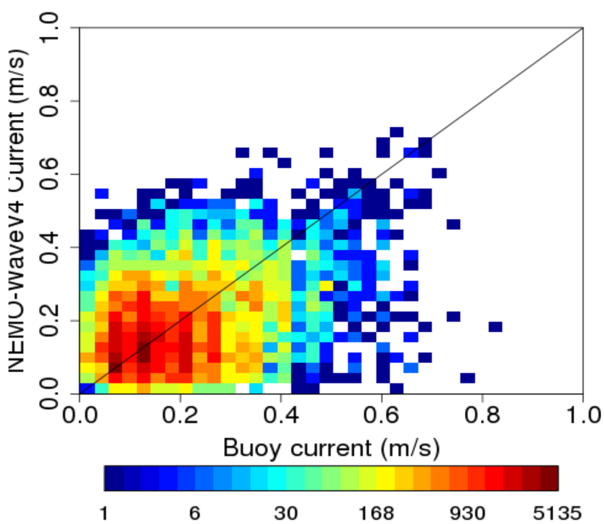

Figure 11 : Scatter plot of surface currents velocity of model and observations at GCan locations during 2014. (a) and (b) indicate runs NEMO-Ref and NEMO-WaveV4,respectively.

Ocean Sci. Discuss., https://doi.org/10.5194/os-2018-167
Manuscript under review for journal Ocean Sci.
Discussion started: 15 February 2019

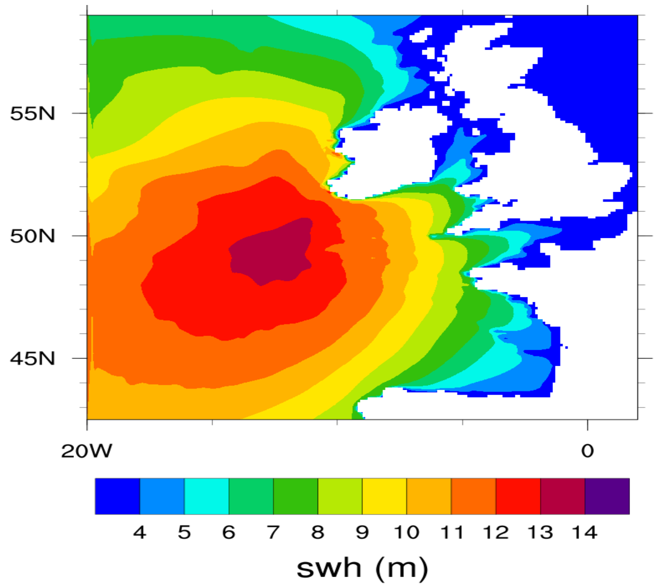

Figure 12 : Significant wave height (m) for 6th January during Storm Hercules.

Ocean Sci. Discuss., https://doi.org/10.5194/os-2018-167
Manuscript under review for journal Ocean Sci.
Discussion started: 15 February 2019

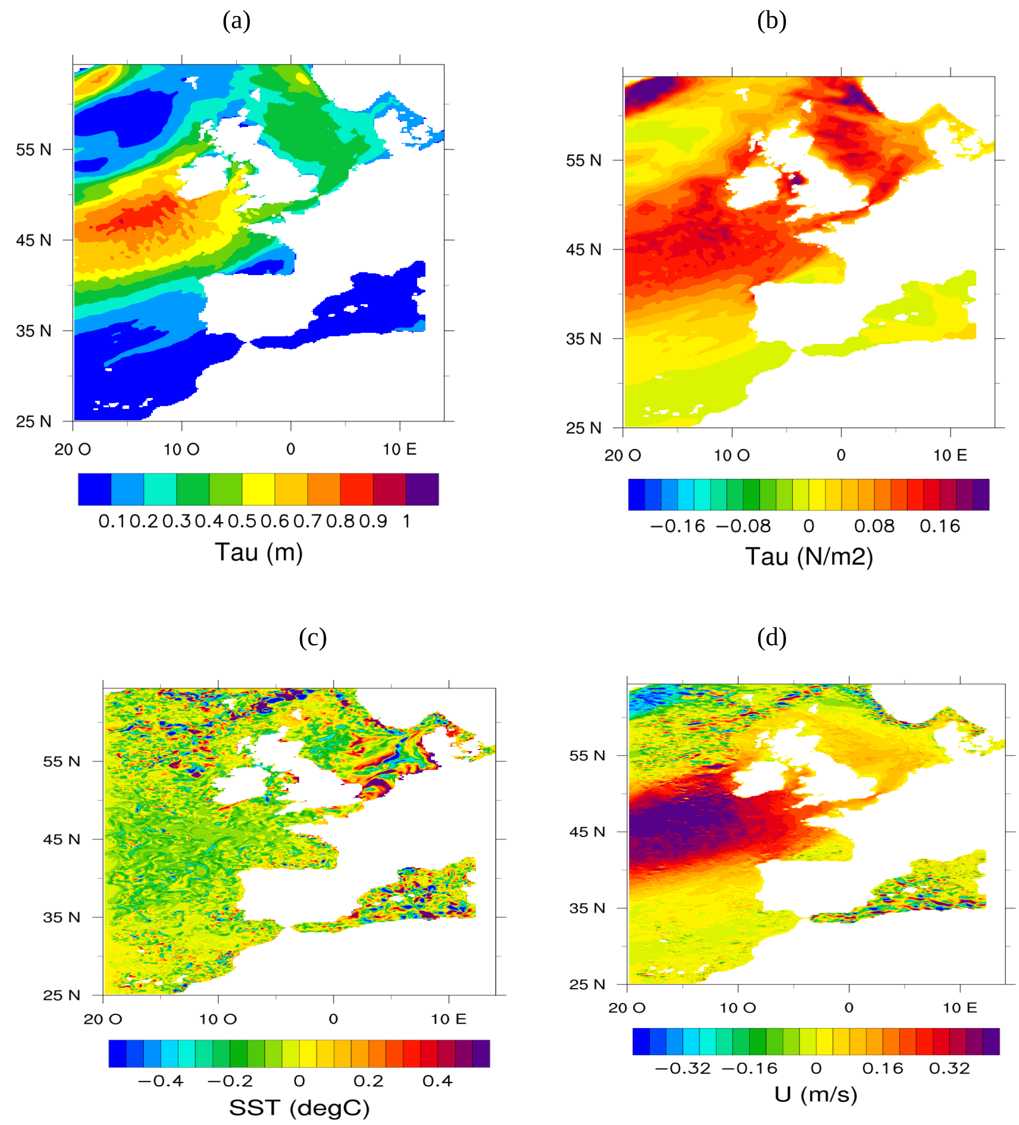

Figure 13 : Daily output for Storm Hercules (6th January 2014) of wind stress of NEMO-Ref (a), difference between NEMO-WaveV4 and NEMO-Ref of wind stress (b), SST (c) and U-component of surface current (d).

Ocean Sci. Discuss., https://doi.org/10.5194/os-2018-167
Manuscript under review for journal Ocean Sci.
Discussion started: 15 February 2019

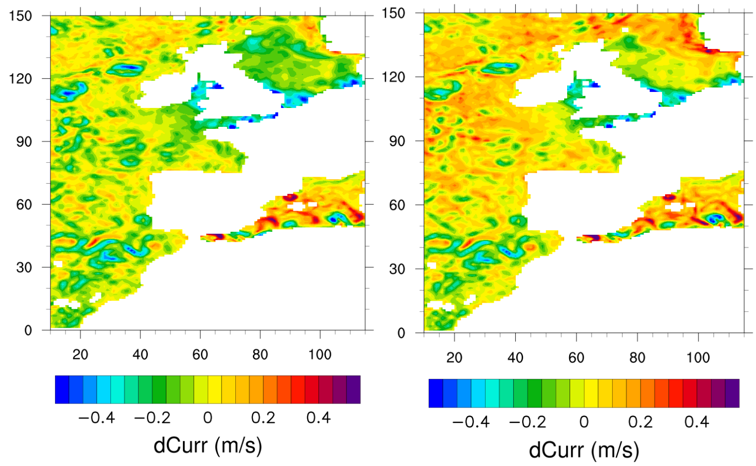

(a) (b)

Figure 14 : Averaged January differences between (a) NEMO-Ref and L4 satellite current and (b) NEMO-WaveV4 and L4 satellite, including Hercules storm (06/01/2014) for surface current velocity.

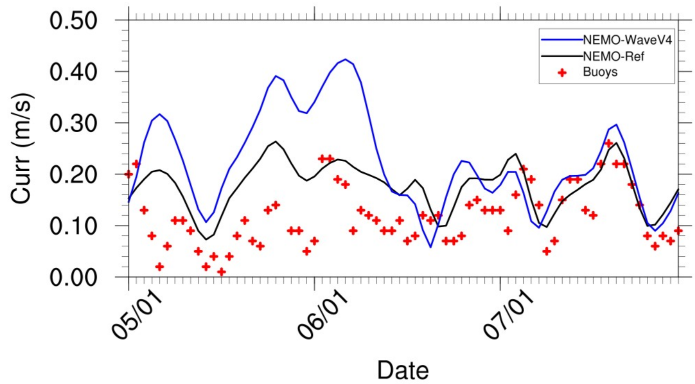

Figure 15 : Time series of surface current at Csil location from 5th until 7th January 2014 during storm Hercules. Red cross, blackand blue lines indicate observations, NEMO-Ref and NEMO-WaveV4.

Ocean Sci. Discuss., https://doi.org/10.5194/os-2018-167
Manuscript under review for journal Ocean Sci.
Discussion started: 15 February 2019

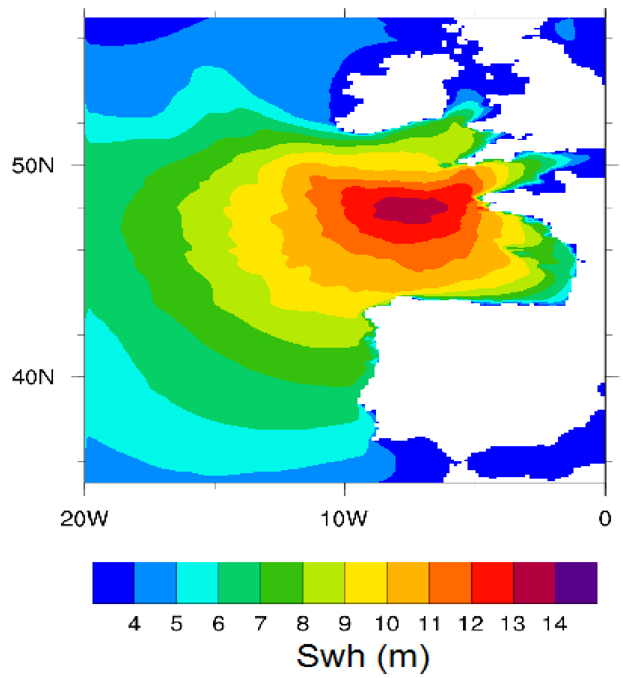

Figure 16 : Significant wave height in meters on 5th February 2014 during storm Petra.

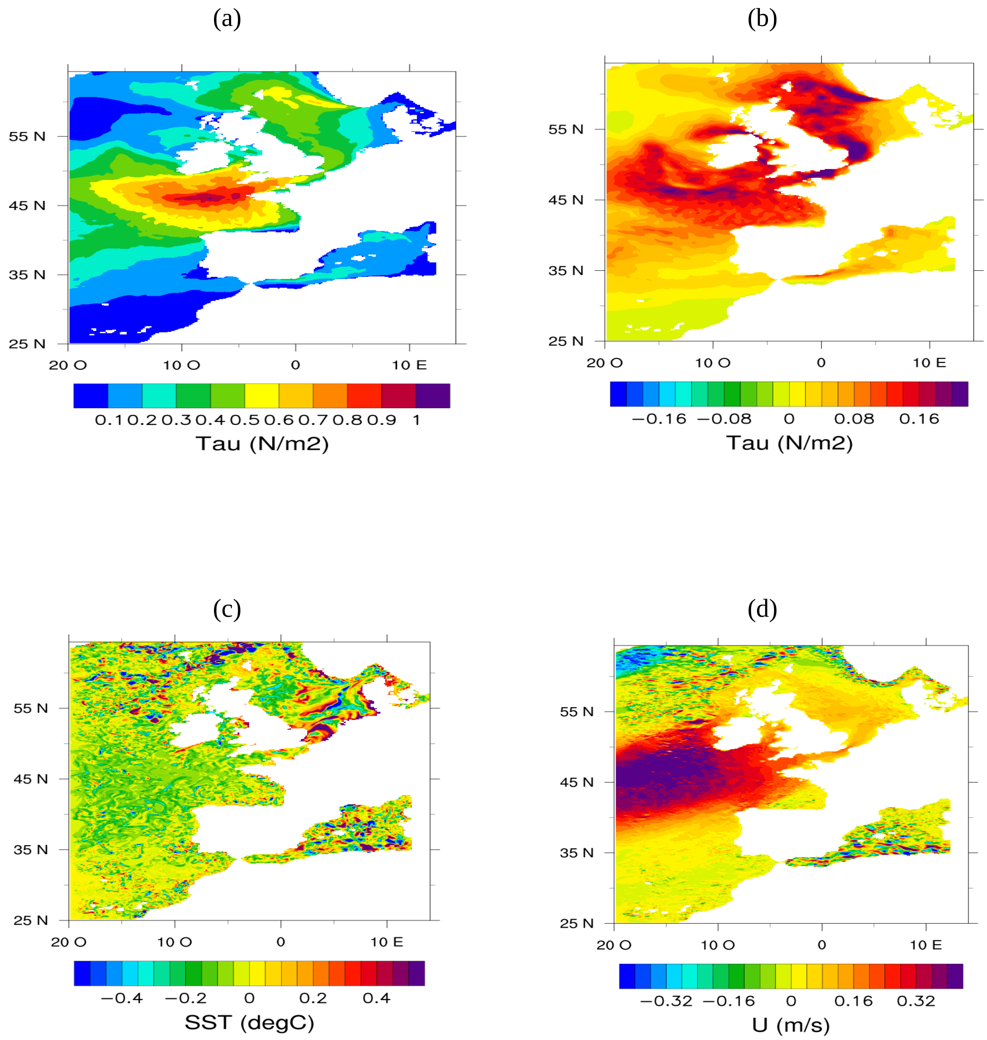

Figure 17 : Daily output during storm Petra on 5th February 2014. (a) indicate the surface stress from run of NEMO-Ref. (b), (c) and (d) show the difference between NEMO-WaveV4 and NEMO-Ref for surface stress, SST and U-component of surface current, respectively.

Ocean Sci. Discuss., https://doi.org/10.5194/os-2018-167
Manuscript under review for journal Ocean Sci.
Discussion started: 15 February 2019

(a)

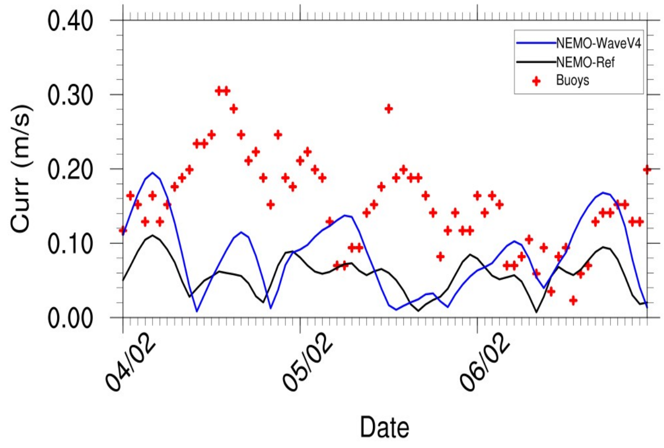

(b)

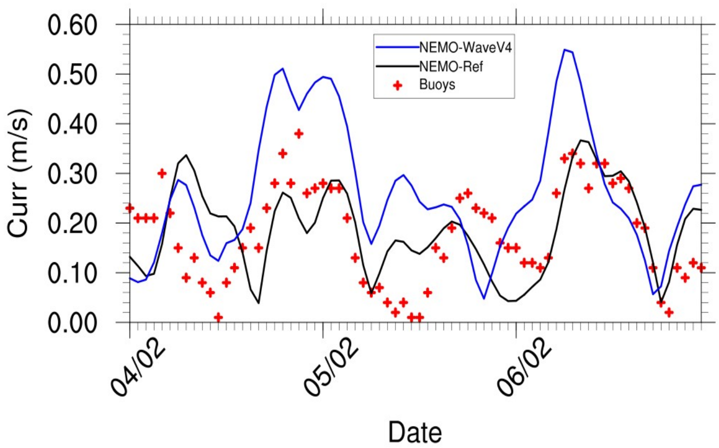

Figure 18 : Time series of surface current from 4 until 6 February 2014 during storm Petra at Bilb (a) and Csil (b) observations. Red cross, black and blue lines stand for observations, NEMO-Ref and NEMO-WaveV4.

(a)

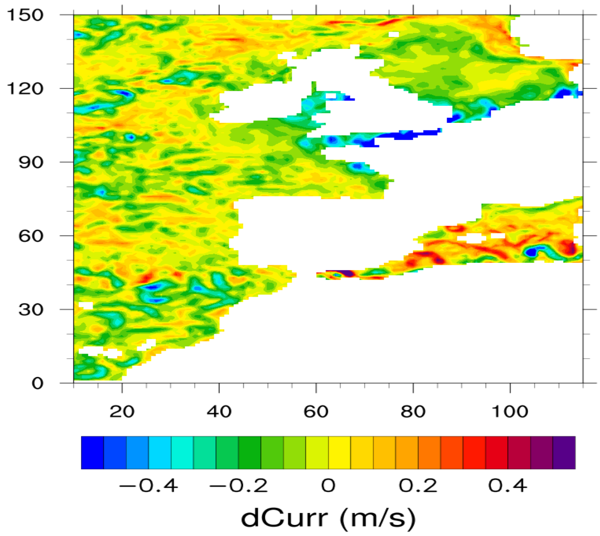

(b)

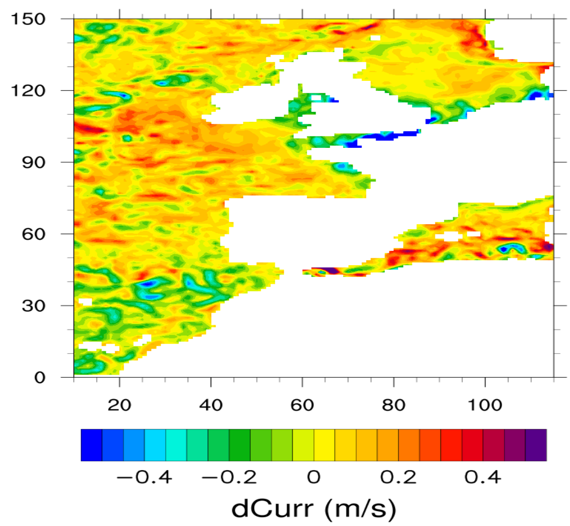

Figure 19 : Averaged differences between NEMO model runs and L4 satellite surface currents during storm Petra on 5 february 2014. (a) and (b) stand for runs NEMO-Ref and NEMO-WaveV4, respectively.

Ocean Sci. Discuss., https://doi.org/10.5194/os-2018-167
Manuscript under review for journal Ocean Sci.
Discussion started: 15 February 2019

Ocean Science
Discussions

(a)

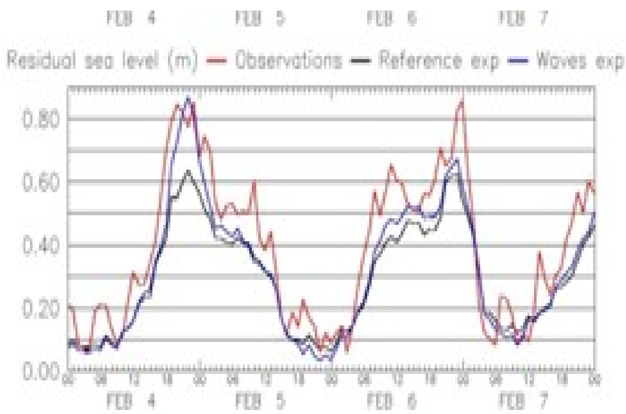

(b)

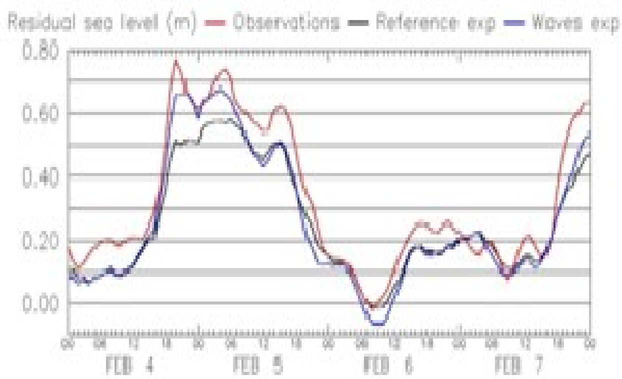

Figure 20 : Time series of sea surface height at Lecrouesty (a) and fishguard (b) locations. Red, black and blue lines indicate observations from tide gages, run from NEMO-Ref and run from NEMO-WaveV4, respectively . at (a) Le Crouesty and (b) Fishguard buoys.

Ocean Sci. Discuss., https://doi.org/10.5194/os-2018-167
Manuscript under review for journal Ocean Sci.
Discussion started: 15 February 2019

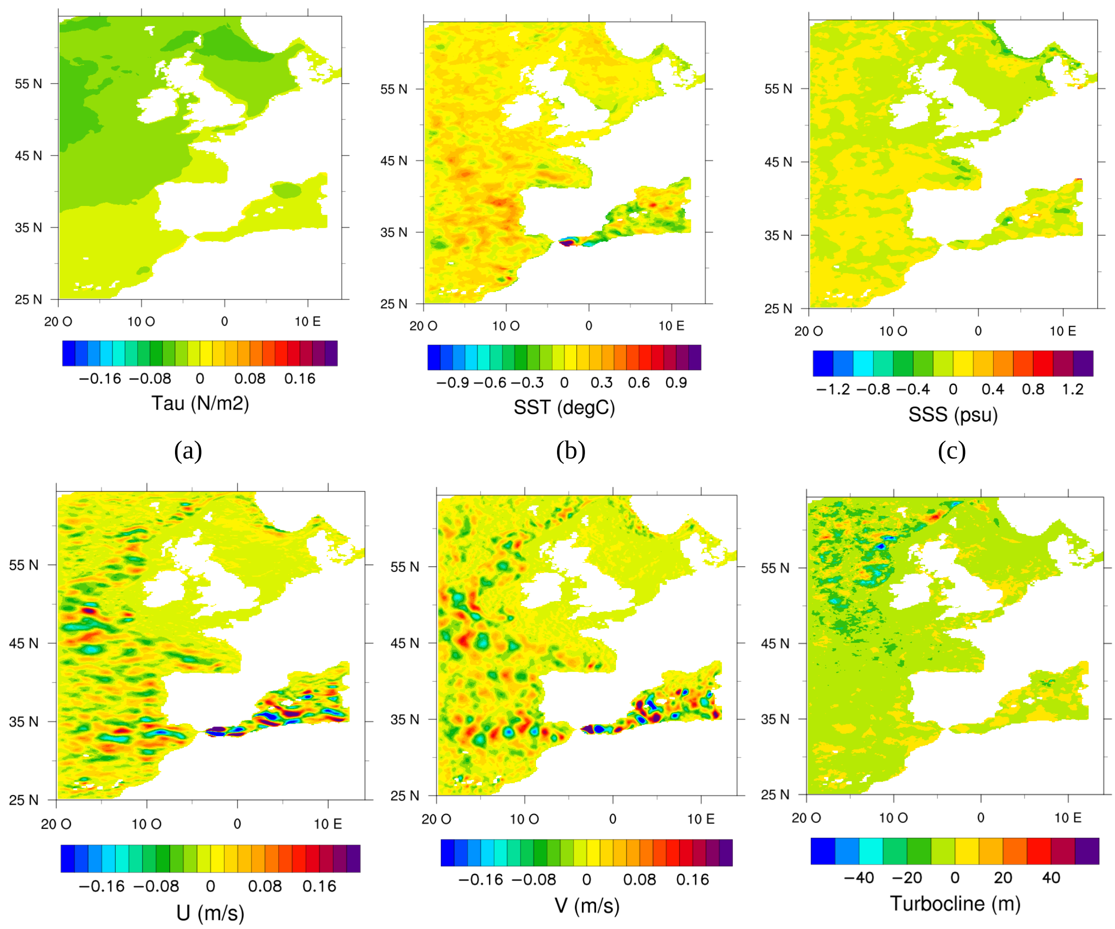

(a) (b) (c)

(d) (e) (f)

Figure 21 : Averaged differences between runs NEMO-WaveV4 and NEMO-WaveV4-NoAtm. (a), (b), (c), (d), (e) and (f) stand for wind stress in N/m^2, SST in °C, SSS in psu, U and V components of surface current in m/s, and Turbocline in m, respectively.

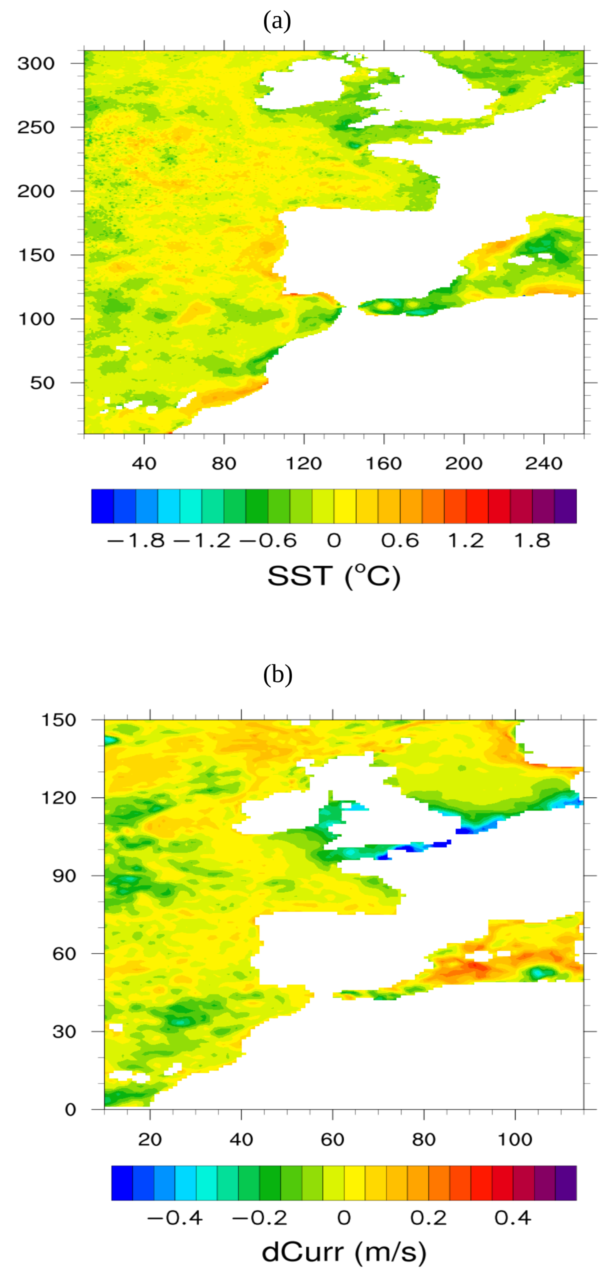

Figure 22 : Mean difference during 2014 from the run NEMO-WaveV4-NoAtm. (a) and (b) stand for the comparison with SST from Level 4 OSTIA and Level 4 surface currents, respectively.

Ocean Sci. Discuss., https://doi.org/10.5194/os-2018-167
Manuscript under review for journal Ocean Sci.
Discussion started: 15 February 2019

Buoy name	Location	Reference code	Nationality
Bilbao Vizcaya	43.64°N 3.05°W	Bilb	Spanish
Cabo de Gata	36.57°N 2.32°W	CGat	Spanish
Cabo de Palos	37.67°N 0.33°W	CPal	Spanish
Cabo Penhas	43.75°N 6.16°W	CPen	Spanish
Cabo Silleiro	42.12°N 9.43°W	CSil	Spanish
Drogonera	39.56°N 2.10°E	Drog	Spanish
Estaca Bares	44.12°N 7.67°W	EBar	Spanish
Golfo de Cadiz	36.48°N 6.96°W	GCad	Spanish
Gran Canaria	28.20°N 15.80°W	GCan	Spanish
Tarragona	40.68°N 1.47°E	Tarr	Spanish
Tenerife	27.99°N 16.58°W	Tene	Spanish
Valencia	39.52°N 0.21°E	Vale	Spanish
Villano Sisargas	43.3°N 9.12°W	Vill	Spanish
Santander	43.50°N 3.46°W	Sant	Spanish
Belle Ile	47.30°N 3.30°W	BI	French
Pierre Noire	48.30°N 5.00°W	PN	French
Plateau du Four	47.20°N 2.80°W	PF	French
Belmullet A	54.28°N 10.27°W	BelmA	Irish
Belmullet B	54.23°N 10.14°W	BelmB	Irish

Table 1 : Name, location, nationality and reference code of the moored buoys.

	NEMO-Ref	NEMO-WaveV4	NEMO-WaveV3
OSTIA Bias (°C), (%)	-0.08 (-0.6%)	-0.12 (-0.8%)	-0.15 (-1.0%)
OSTIA RMS (°C), (%)	0.27 (1.4%)	0.25 (1.3%)	0.26 (1.3%)
L3S Bias (°C), (%)	-0.24 (-1.4%)	-0.30 (-1.8%)	-0.32 (-1.9)
L3S RMS (°C), (%)	0.30 (2.0%)	0.30 (2.0%)	0.30 (2.0%)

Table 2 : Scores between NEMO SST and SST satellite products OSTIA and L3S.

Ocean Sci. Discuss., https://doi.org/10.5194/os-2018-167
Manuscript under review for journal Ocean Sci.
Discussion started: 15 February 2019

	Bias (m/s) (%)	RMS (m/s) (%)
NEMO-Ref	-0.05 (- 26.8 %)	0.08 (41.2 %)
NEMO-WaveV4	-0.02 (-12.5 %)	0.07 (39.2 %)
NEMO-WaveV3	-0.03 (-16.8 %)	0.07 (39.2 %)

Table 3 : Scores for 2014 between NEMO experiments and L4 currents for surface current velocity.

	Current Module			
	Bias (m/s) (%Bias)		**RMS (m/s) (%RMS)**	
	NEMO-Ref	**NEMO-WaveV4**	**NEMO-Ref**	**NEMO-WaveV4**
Bilb	0.01 (3.6%)	0.02 (7.8%)	0.09 (61.1%)	0.08 (58.6%)
CGat	-0.01 (-1.0%)	0.08 (42.3%)	0.11 (56.1%)	0.16 (82.3%)
CPal	0.32 (181.5%)	0.25 (138.3%)	0.33 (186.3%)	0.28 (159.6%)
CPen	0.04 (29.3%)	0.06 (46.8%)	0.09 (76.5%)	0.11 (86.2%)
CSil	0.01 (5.3%)	0.02 (19.5%)	0.05 (52.5%)	0.06 (57.6%)
Cadi	-0.01 (-2.9%)	-0.03 (-17.1%)	0.08 (41.2%)	0.07 (40.9%)
Drog	0.05 (38.5%)	0.06 (48.8%)	0.11 (88.7%)	0.10 (77.9%)
EstB	0.04 (37.4%)	0.05 (49.9%)	0.08 (76.3%)	0.09 (81.9%)
GCan	-0.06 (-37.3%)	-0.04 (-24.4%)	0.10 (64.6%)	0.09 (55.9%)
Sant	0.01 (-4.0%)	0.01 (4.0%)	0.08 (57.4%)	0.09 (68.5%)
Tarr	0.00 (0.0%)	-0.03 (14.4%)	0.09 (45.7%)	0.10 (50.5%)
Tene	-0.01 (-7.9%)	-0.03 (-23.4%)	0.09 (76.0%)	0.08 (70.0%)
Vale	0.01 (11.6%)	0.03 (32.9%)	0.07 (70.8%)	0.08 (81.7%)
Vill	0.06 (51.8%)	0.09 (79.8%)	0.08 (76.9%)	0.10 (93.8%)

Table 4 : Bias and RMS error during 2014 between buoy observations and NEMO-Ref/NEMO-WaveV4 for surface currents at the moored buoys showed in Table 1 and Figure 1.

	NEMO-Ref		NEMO-WaveV4	
	Bias (m/s) (%)	**RMS (m/s) (%)**	**Bias (m/s) (%)**	**RMS (m/s) (%)**
L4 satellite	-0.06 (-28.7%)	0.11 (54.0%)	0.01 (0.7%)	0.11 (54.0%)
CSil	0.06 (49.6%)	0.07 (56.8%)	0.11 (89.5%)	0.12 (97.9 %)
EBar	0.06 (19.6%)	0.12 (40.8%)	0.14 (47.2%)	0.17 (56.1%)
Vill	0.19 (225.6%)	0.21 (245.9%)	0.33 (388.9%)	0.33 (388.9%)

Table 5 : Scores for surface current during Storm Hercules (06/01/2014) in comparison with L4 satellite and moored buoys impacted by storm for NEMO-Ref and NEMO-WaveV4.

	NEMO-Ref		NEMO-WaveV4	
	Bias (m/s) (%)	**RMS (m/s) (%)**	**Bias (m/s) (%)**	**RMS (m/s) (%)**
L4 current	-0.05 (-26.8%)	0.10 (53.4%)	0.01 (4.0%)	0.11 (56.6%)
Bilb	-0.10 (-63.0%)	0.10 (63.0%)	-0.07 (-44.5%)	0.09 (58.5%)
CSil	0.01 (4.8%)	0.08 (43.9%)	0.09 (49.2%)	0.13 (73.2%)
EBar	0.07 (38.4%)	0.14 (73.6%)	0.11 (59.4%)	0.16 (85.0%)

Table 6 : Scores for surface current during Storm Petra (6^{th} February 2014) on IBI domain in comparisons with L4 currents and at the impacted moored buoys for NEMO-Ref and NEMO-WaveV4.

	NEMO-Ref	NEMO-WaveV4	NEMO-WaveV4-NoAtm
OSTIA Bias (°C), (%)	-0.08 (-0.6%)	-0.12 (-0.8%)	-0.06 (-0.4%)
OSTIA RMS (°C), (%)	0.27 (1.4%)	0.25 (1.3%)	0.27 (1.4%)
L3S Bias (°C), (%)	-0.24 (-1.4%)	-0.30 (-1.8%)	-0.22 (-1.3%)
L3S RMS (°C), (%)	0.30 (2.0%)	0.30 (2.0%)	0.29 (1.8%)
L4 Current Bias (m/s), (%)	-0.05 (-26.8%)	-0.02 (-12.5%)	-0.03 (-16.0%)
L4 Current RMS (m/s), (%)	0.08 (41.2%)	0.07 (39.2%)	0.07 (39.2%)

Table 7 : Scores for NEMO-Ref, NEMO-WaveV4 and NEMO-WaveV4-NoAtm during 2014 of the comparisons with OSTIA and L3S SST.